Connected Vehicle Experiments on Virtual Rings: Unveiling Bistable Behavior

Bence Szaksz, Tamas G. Molnar, Sergei S. Avedisov, Gábor Stepan, and Gábor Orosz

***Abstract*—The nonlinear dynamics of vehicles on a virtual ring is investigated. A vehicle chain is considered where a connected automated vehicle (CAV) driving at the head of the chain receives the state of a connected human-driven vehicle (CHV) at the tail. The controller of the CAV is constructed in a way that the CHV is projected in front of it; this closes a virtual ring. We construct the corresponding mathematical model and analyze the effect of nonlinearities with numerical continuation. Then, we present real car experiments with two CHVs and one CAV. Both the theoretical results and the experiments show bistable behavior for certain control parameters. The results provide an essential support for parameter tuning during the control design of CAVs.**

***Index Terms*—Connected automated vehicles, traffic flow, vehicles on a virtual ring.**

I. Introduction

Advanced driver assistance systems have been improving the safety and driving comfort of individual vehicles. However, improving the overall behavior of traffic to prevent the formation of phantom traffic jams [1], [2] remains a challenge on heavily used highways. Vehicle-to-everything (V2X) communication [3] can help to tackle this problem. V2X connectivity enables connected automated vehicles (CAVs) to receive and respond to information about other vehicles in traffic. This led to the concept of cooperative adaptive cruise control [4]–[6] where multiple CAVs are connected to each other, and to the concepts of connected cruise control [7]–[9] and connected traffic control [10], [11] where a CAV receives information from connected human-driven vehicles (CHVs) ahead/behind.

A relatively large number of vehicles are required to form congestion in open vehicle chains. While this is the case in real-world scenarios, it makes it challenging to experimentally study traffic jams with just a few vehicles. The number of vehicles can be reduced by adding a periodic boundary condition and analyzing the dynamics of vehicles on a ring [12]–[14].

The experimental realization of the ring configuration faces significant challenges. The ring needs to be large enough so that the lateral dynamics can be neglected and the drivers can focus on car-following. For example, in the experiments in [12], [15], rings with radii of about 40 meters were used with 22 vehicles. Still, the speed had to be kept low to limit the lateral acceleration: a maximum lateral acceleration of about $3.5\,\mathrm{m/s^2}$, corresponding to the comfort level of human drivers, requires the speed to be below $12\,\mathrm{m/s}$. This speed range is much lower than the one experienced on highways.

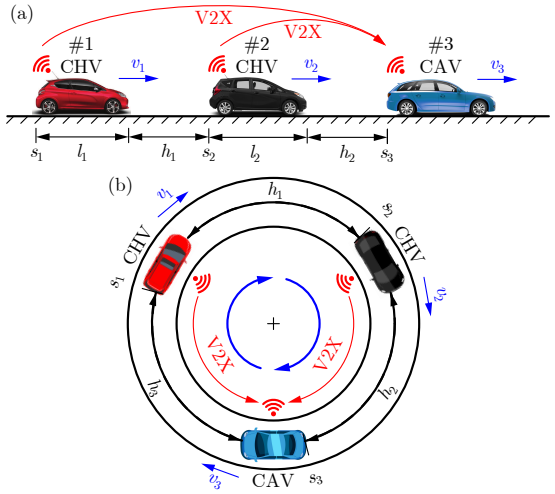

Fig. 1. The concept of virtual ring for three vehicles. The head connected automated vehicle (CAV) responds to the connected human-driven vehicles (CHVs) behind while it pretends to follow the tail CHV on the virtual ring.

To overcome this challenge, we put forward the concept of *virtual ring* [3], [10], where the vehicles drive on a straight road such that a CAV travels at the head of a vehicle chain and a CHV travels at the tail. Using V2X communication, the CAV responds to the CHV as if the CHV was driving ahead of the CAV. By "projecting the CHV ahead", the CAV closes the virtual ring. This enables us to carry out experiments at real highway speeds, without subjecting the drivers to lateral acceleration. Such experiments are utilized to reveal nonlinear phenomena, referred to as bistability, behind the formation of phantom jams on highways. As [10] was limited to simulation-based analysis, the present study provides the first real-world validation of bistability occurring in virtual rings. The experiments also serve as benchmark for evaluating different connectivity-based control strategies in mixed traffic scenarios where CAVs interact with human-driven vehicles.

The paper is organized as follows. Section II discusses the concept of the virtual ring and introduces the control strategies of human-driven and connected automated vehicles. Then, the nonlinear analysis of the system is carried out in Sec. III. In Sec. IV, the theoretical results are validated by real-life experiments with three vehicles, including a CAV. Finally, we add some concluding remarks in Sec. V.

Bence Szaksz is with the Department of Applied Mechanics, and with the MTA-BME Lendulet "Momentum" Global Dynamics Research Group, Budapest University of Technology and Economics, Budapest, H-1111, Hungary. szaksz@mm.bme.hu.

Tamas G. Molnar is with the Department of Mechanical Engineering, Wichita State University, Wichita, KS 67260, USA. tamas.molnar@wichita.edu.

Sergei S. Avedisov is with the Department of Mechanical Engineering, University of Michigan, Ann Arbor, MI 48109, USA. avediska@umich.edu.

Gábor Stepan is with the Department of Applied Mechanics, and with the HUN-REN–BME Dynamics of Machines Research Group, Budapest University of Technology and Economics, Budapest, H-1111, Hungary. stepan@mm.bme.hu.

Gábor Orosz is with the Department of Mechanical Engineering and with the Department of Civil and Environmental Engineering, University of Michigan, Ann Arbor, MI 48109, USA. orosz@umich.edu.

II. Modeling

Figure 1 depicts the virtual ring configuration for three vehicles. The blue CAV drives at the head of a vehicle chain while it pretends to follow the red CHV at the tail. Such configuration is enabled by V2X communication which allows the CAV to respond to multiple vehicles "ahead". In the example shown, the red vehicle is "immediately ahead" of the blue vehicle while the black vehicle is "two vehicles ahead". This setup enables vehicles to drive at realistic speed and facilitates the study of their behavior at nonlinear level.

The realization of the virtual ring requires the definition of the headway of the CAV. Consider that N vehicles are placed on a (virtual) ring of length $L + Nl$ where L is the net ring length and l is the length of the vehicles (considered to be the same for all vehicles for simplicity). We number the vehicles from the tail CHV to the head CAV as $i = 1, \dots, N$, see Fig. 1(a) for $N = 3$. The headway and the velocity of the i-th vehicle are denoted by h_i and v_i, respectively. The sum of the headways gives the net ring length which allows us to express the CAV's headway as

$$\sum_{i=1}^{N} h_i = L \quad \Rightarrow \quad h_N = L - \sum_{i=1}^{N-1} h_i \,. \tag{1}$$

The equation of motion takes the form

$$\dot{h}_i(t) = v_{i+1}(t) - v_i(t)\,, \quad \text{for } i \in \{1, \dots, N-1\}\,, \tag{2}$$

$$\dot{v}_i(t) = \mathrm{sat}(u_i(t - \tau_i))\,, \quad \text{for } i \in \{1, \dots, N\}\,, \tag{3}$$

where τ_i is the delay in the control of the i-th vehicle, while

$$\mathrm{sat}(u) = \begin{cases} u_{\min}, & \text{if } u < u_{\min}\,, \\ u, & \text{if } u_{\min} \le u \le u_{\max}\,, \\ u_{\max}, & \text{if } u > u_{\max}\,. \end{cases} \tag{4}$$

Note that the CAV's headway is not presented in (2) since it is obtained from the geometric constraint (1). In the following numerical analysis, the minimum and maximum accelerations are $u_{\min} = -7\,\mathrm{m/s^2}$, and $u_{\max} = 3\,\mathrm{m/s^2}$, respectively.

The human driving behavior is approximated by the optimal velocity model [16], [17] as

$$u_i = \alpha_i\big(V_i(h_i) - v_i\big) + \beta_i\big(W_i(v_{i+1}) - v_i\big)\,, \tag{5}$$

with the parameters α_i and β_i, the nonlinear range policy function

$$V_i(h) = \begin{cases} 0, & \text{if } h < h_{\mathrm{st},i}\,, \\ v_{\max,i}\left(1 - \left(\frac{h_{\mathrm{go},i} - h}{h_{\mathrm{go},i} - h_{\mathrm{st},i}}\right)^2\right), & \text{if } h_{\mathrm{st},i} \le h \le h_{\mathrm{go},i}\,, \\ v_{\max,i}, & \text{if } h > h_{\mathrm{go},i}\,, \end{cases} \tag{6}$$

and the speed policy

$$W_i(v) = \begin{cases} v\,, & \text{if } v < v_{\max,i}\,, \\ v_{\max,i}\,, & \text{if } v \ge v_{\max,i}\,. \end{cases} \tag{7}$$

The range policy functions V_i imply that the drivers aim to stop if their headway is smaller than a prescribed value, i.e., $h \le h_{\mathrm{st}}$, while they aim to keep a maximum velocity $v_{\max}$ if the vehicle ahead is far enough, i.e., $h \ge h_{\mathrm{go}}$. In between, we consider a smooth second-order function.

The controller of the CAV is also designed based on the optimal velocity model with the "trick" that the CHV #1 is projected in front of the CAV in a distance of h_N; cf. (1). The corresponding controller is given in the form

$$u_N = \alpha_N\big(V_N(h_N) - v_N\big) + \beta_N\big(W_N(v_1) - v_N\big)\,, \tag{8}$$

with gains α_N, β_N and the piecewise linear range policy

$$V_N(h) = \begin{cases} 0, & \text{if } h < h_{\mathrm{st},N}\,, \\ v_{\max,N}\frac{h - h_{\mathrm{st},N}}{h_{\mathrm{go},N} - h_{\mathrm{st},N}}, & \text{if } h_{\mathrm{st},N} \le h \le h_{\mathrm{go},N}\,, \\ v_{\max,N}, & \text{if } h > h_{\mathrm{go},N}\,, \end{cases} \tag{9}$$

while the speed policy W_N takes the same form as in (7).

Model (1)-(9) captures the following behaviors. It has an equilibrium, where all vehicles travel with the same constant velocity and keep constant headways that are determined by the range policies. If the equilibrium is stable, the effects of perturbations (like a braking of an individual driver) vanish over time and smooth traffic is observed. If the equilibrium is unstable, the velocities start to oscillate, which corresponds to repeated slowdowns in traffic jams. We use DDE-BIFTOOL [18] to numerically analyze the (local and global) stability of the equilibrium and the occurrence of periodic oscillations (limit cycles) for the nonlinear dynamics (1)-(9). We remark that nonlinearities and time delays make it particularly challenging to identify and control dynamics [19]–[21].

III. Numerical analysis

Consider that the CAV travels in front of two human-driven vehicles (HVs), the second of which is a CHV. The net length of the virtual ring is $L = 75\,\mathrm{m}$. For the sake of simplicity, assume that the human drivers are identical and their behavior is described by the parameters $h_{\mathrm{st,h}} = 5\,\mathrm{m}$, $h_{\mathrm{go,h}} = 35\,\mathrm{m}$, $v_{\max,\mathrm{h}} = 22\,\mathrm{m/s}$, $\alpha_{\mathrm{h}} = 0.25\,\mathrm{s^{-1}}$, and $\tau_{\mathrm{h}} = 1\,\mathrm{s}$. The parameters of the CAV are $h_{\mathrm{st},N} = 5\,\mathrm{m}$, $v_{\max,N} = 30\,\mathrm{m/s}$, $\alpha_N = 0.4\,\mathrm{s^{-1}}$, $\beta_N = 0.5\,\mathrm{s^{-1}}$, and $\tau_N = 0.6\,\mathrm{s}$.

Figure 2(a) presents a stability chart that shows the stability of the equilibrium for various values of the CAV's free flow headway $h_{\mathrm{go},N}$ and the HVs' control gain β_{h}. The equilibrium is stable in the union of the shaded domains. Along the stability boundaries, shown by black lines, Hopf bifurcation occurs and the system loses its stability with oscillations. Analyzing the nonlinear dynamics reveals two qualitatively different behaviors in the shaded domain. In the gray region, the equilibrium is globally stable, and speed fluctuations decay for arbitrary perturbations, which leads to smooth traffic. In the brick-colored bistable domain, stable limit-cycles coexist with the stable equilibrium. At these parameter combinations, the system converges to the equilibrium for small perturbations, and large enough perturbations result in oscillatory motions. That is, a large enough braking of a driver may trigger oscillations in vehicle speeds, similar to those in traffic jams.

Panels (b), (c), (e) and (f) show bifurcation diagrams for fixed values of the free flow headway $h_{\mathrm{go},N}$ obtained with

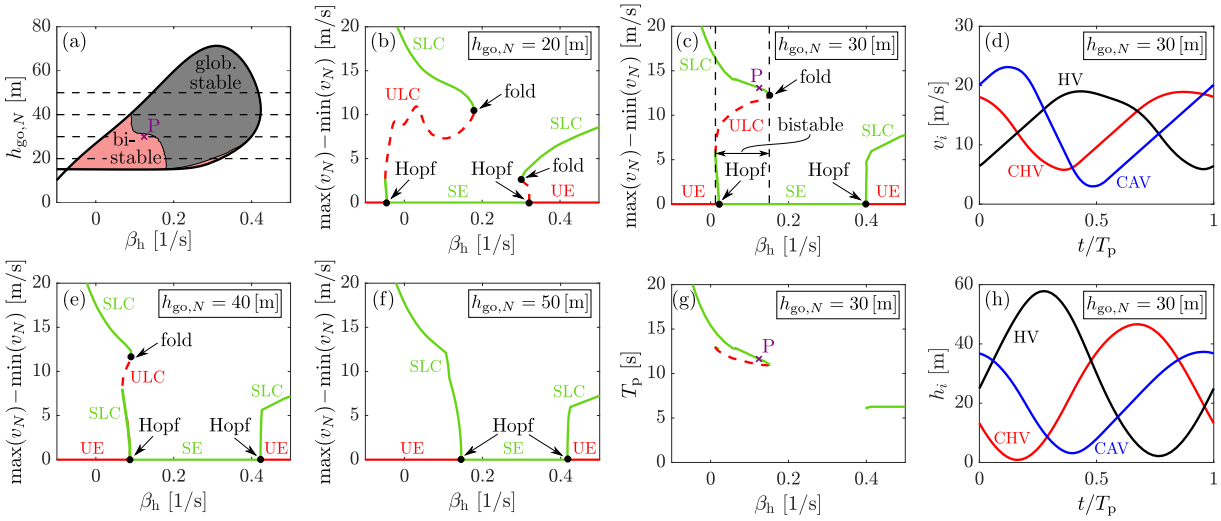

Fig. 2. Nonlinear analysis of the dynamics (1)-(9) on a virtual ring with $N = 3$ vehicles. Panel (a) presents a stability chart, while panels (b), (c), (e) and (f) are bifurcation diagrams for various values of the free flow headway $h_{\mathrm{go},N}$. Panel (h) depicts the time period of oscillation of the limit cycles existing for $h_{\mathrm{go},N} = 30\,\mathrm{m}$. Finally, panels (d) and (h) visualize the stable limit cycles for $h_{\mathrm{go},N} = 30\,\mathrm{m}$ and $\beta_{\mathrm{h}} = 0.12\,\mathrm{s}^{-1}$ (see point P in (a), (c) and (g)).

DDE-BIFTOOL [18]. The diagrams show branches of unstable equilibria (UE) and stable equilibria (SE). These are separated by Hopf bifurcation points, which give rise to branches of unstable limit cycles (ULC) and stable limit cycles (SLC). For $h_{\mathrm{go},N} = 20\,\mathrm{m}$ and $h_{\mathrm{go},N} = 30\,\mathrm{m}$, the branch emerging from the left Hopf point turns right, then a fold bifurcation occurs, and the branch turns back to the left. The range of β_{h} values between the Hopf and fold points, where SE and SLC coexist, is called a bistable domain; see panel (c). The bistable domain shrinks and disappears as the parameter $h_{\mathrm{go},N}$ increases.

Panel (g) presents the time period T_{p} of oscillation for the limit cycles obtained for $h_{\mathrm{go},N} = 30\,\mathrm{m}$. It is about 12 s at the fold point of the left branch and it increases with the increase of the limit cycle amplitude. Meanwhile, the time period of oscillation of the right limit cycle is about 6 s.

Panels (d) and (h) show the time evolution of the velocities and headways for the stable limit cycle at $h_{\mathrm{go},N} = 30\,\mathrm{m}$ and $\beta_{\mathrm{h}} = 0.12\,\mathrm{s}^{-1}$ (see point P in panels (a), (c) and (g)). The CAV performs large (saturated) accelerations and decelerations, while its headway gets relatively small. This helps the human drivers, since they can keep longer headways along the ring.

We repeated the analysis for a virtual ring with $N = 6$ vehicles in Fig. 3, using the same parameters as before except for $\alpha_{\mathrm{h}} = 0.15\,\mathrm{s}^{-1}$ and $\tau_{\mathrm{h}} = 0.9\,\mathrm{s}$. Figure 3(a) shows that, in this case, almost the entire linearly stable region is bistable.

Figure 3(b) shows that, for $h_{\mathrm{go},N} = 20\,\mathrm{m}$, the two branches of limit cycles emerging from the left and right Hopf points are still separated, and the fold points are located such that there always exists a SLC above the SE. As $h_{\mathrm{go},N}$ is increased, the two branches meet and create a gate-like branch of ULC above the equilibrium, and an isolated branch of large-amplitude SLC; see panel (c). As panel (e) depicts, a further increase of $h_{\mathrm{go},N}$ yields that the branches meet and separate again to left and right branches. In this configuration, a bistable and a globally stable interval exist, which is consistent with the stability chart in panel (a). Panel (f) illustrates that, for $h_{\mathrm{go},N} = 52\,\mathrm{m}$, again, a gate-like unstable branch is above the SE, while a large amplitude isolated stable branch also exists.

The corresponding time period of oscillations in panel (g) is larger than in the $N = 3$ case, which can be explained by the fact that more vehicles are involved in the oscillation.

Finally, panels (d) and (h) present the velocities and the headways as a function of the normalized time for the SLC at $h_{\mathrm{go},N} = 30\,\mathrm{m}$ and $\beta_{\mathrm{h}} = 0.35\,\mathrm{s}^{-1}$ (see point P in panels (a), (c) and (g)). Again, the CAV performs large accelerations and decelerations, which allows keeping relatively small headway.

IV. Virtual Ring Experiments

We also conducted experiments to demonstrate the applicability of the theoretical results. The experiments utilized two CHVs and one CAV, all equipped with a V2X kit, which includes a V2X on-board unit (OBU), an antenna for GPS and V2X communication, and a laptop. The OBU is connected to the laptop via Ethernet and powered by a 12V supply through the vehicle's cigar lighter. Using this setup, the vehicles were able to share motion information with each other. The shared data included GPS position, GPS-based speed, and heading angle, all transmitted at a 10 Hz update rate. The CAV was a commercial vehicle that was modified to enable control over its longitudinal and lateral motions.

In practice, the positions s_i of the vehicles are not determined individually but rather the distances $s_i - s_j$ are calculated using the Haversine formula [22] that provides the great circle distance between two points of GPS coordinates. This is used to obtain the distance between the rear bumpers of the head CAV and the tail CHV:

$$s_N - s_1 = \sum_{i=1}^{N-1} h_i + (N-1)l\,, \tag{10}$$

cf. Fig. 1(b) for $N = 3$. Substituting this into (1) results in

$$h_N = L + (N-1)l - (s_N - s_1)\,. \tag{11}$$

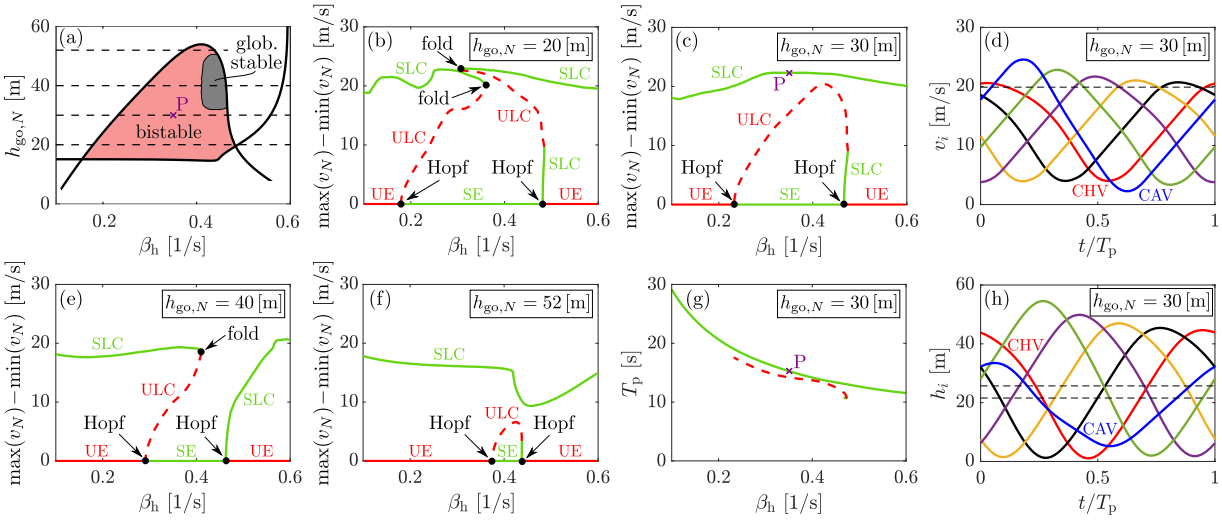

Fig. 3. Nonlinear analysis of the dynamics (1)-(9) on a virtual ring with $N = 6$ vehicles. Panel (a) presents a stability chart, while panels (b), (c), (e) and (f) are bifurcation diagrams for various values of the free flow headway $h_{\mathrm{go},N}$. Panel (h) depicts the time period of oscillation of the limit cycles existing for $h_{\mathrm{go},N} = 30\,\mathrm{m}$. Finally, panels (d) and (h) visualize the stable limit cycles for $h_{\mathrm{go},N} = 30\,\mathrm{m}$ and $\beta_{\mathrm{h}} = 0.35\,\mathrm{s}^{-1}$ (see point P in (a), (c) and (g)).

With the shifted position $s_{N+1} = s_1 + L + Nl$, one obtains

$$h_N = s_{N+1} - s_N - l\,. \tag{12}$$

Note that this can be generalized for vehicles of different lengths with $s_{N+1} = s_1 + L + \sum_{i=1}^{N} l_i$.

For the experimental results presented below, we utilize $N = 3$ vehicles of length $l = 5\,\mathrm{m}$ on a virtual ring of length $L + 3l = 90\,\mathrm{m}$. Figs. 4-7 depict the measured speed, acceleration and headway of all three vehicles in the top, middle and bottom panels, respectively. Observe that the speed reaches $25\,\mathrm{m/s}$, which is a realistic speed for highway driving. If one wanted to carry out these experiments on a physical ring road, lateral accelerations would have reached $43.5\,\mathrm{m/s^2}$, that is, around 4.5 g. This is more than ten times larger than what is considered to be comfortable in normal driving, and only race car drivers can venture into this territory. This demonstrates the necessity of the virtual ring setup.

In Fig. 4, the blue CAV responds to the red CHV "ahead". The speed limit is set to $v_{\max,N} = 30\,\mathrm{m/s}$, the standstill headway is $h_{\mathrm{st},N} = 5\,\mathrm{m}$, and the free flow headway is $h_{\mathrm{go},N} = 55\,\mathrm{m}$. The remaining parameters of the CAV are $\alpha_N = 0.4\,\mathrm{s}^{-1}$ and $\beta_N = 0.5\,\mathrm{s}^{-1}$. After some initial transients, the system approaches an equilibrium where the vehicles maintain the same constant speed and constant (but not uniform) headways. Around $t = 50\,\mathrm{s}$, the red CHV imposes a perturbation by tapping the brake. This perturbation propagates along the virtual ring as the blue CAV and then the black HV respond to it, and thus, it reaches the red CHV again. The consecutive braking events become weaker and weaker, and after these transient oscillations decay, the system returns to the equilibrium. At around $t = 70\,\mathrm{s}$, the CHV applies another perturbation which also leads to transient oscillations. In this case, it takes longer time for the transients to decay but eventually the system returns to the equilibrium. Based on these experiments, one may declare that the equilibrium is

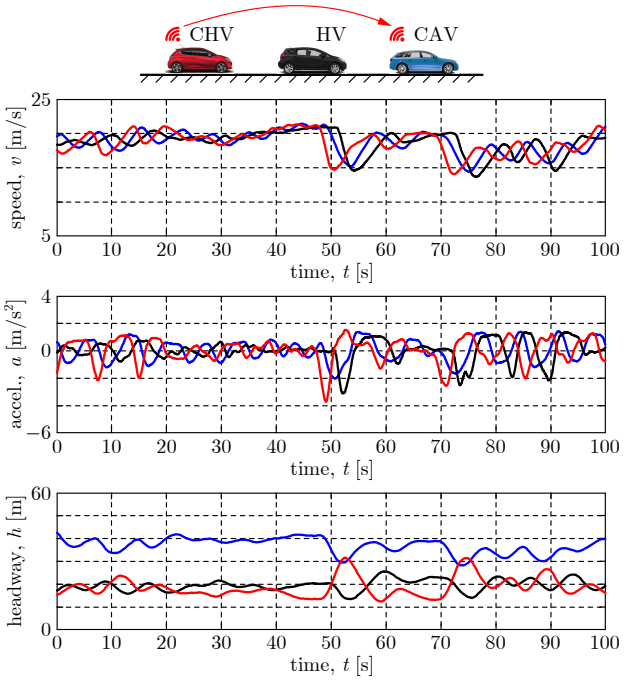

Fig. 4. Virtual ring experiment for virtual ring length $L + 3l = 90\,\mathrm{m}$ where the CAV responds to one CHV "ahead" while utilizing the controller (7,8,9) with free flow headway $h_{\mathrm{go}} = 55\,\mathrm{m}$. The red CHV imposes perturbations around $t = 50\,\mathrm{s}$ and $t = 70\,\mathrm{s}$ and in both cases the system returns to the equilibrium after some transient oscillations.

globally stable for the chosen controller, which we also found to be the case for other values of the net ring length L.

Note that the equilibrium is nonuniform (i.e., the equilibrium headways differ from each other) since the vehicles are not identical. In particular, in Fig. 4, we have $h_1^* \approx h_2^* < h_3^*$, that is, the CAV maintains a larger headway compared to those of the human drivers.

In Fig. 5, the same control strategy is used as in Fig. 4, i.e.,

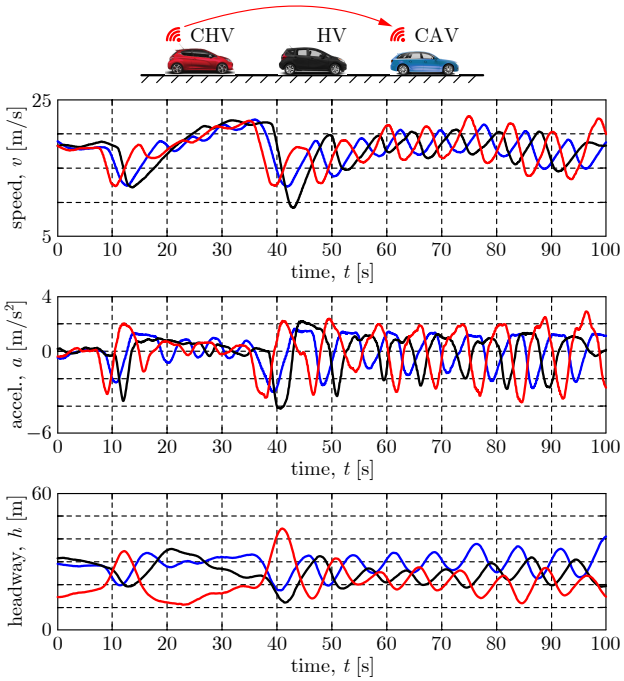

Fig. 5. Virtual ring experiment for virtual ring length $L + 3l = 90\,\mathrm{m}$ where the CAV responds to one CHV "ahead" while utilizing the controller (7,8,9) with free flow headway $h_{\mathrm{go}} = 42.5\,\mathrm{m}$. The red CHV imposes perturbations around $t = 10\,\mathrm{s}$ and $t = 35\,\mathrm{s}$. In the former case the system returns to the equilibrium while in the latter case limit cycle oscillations develop.

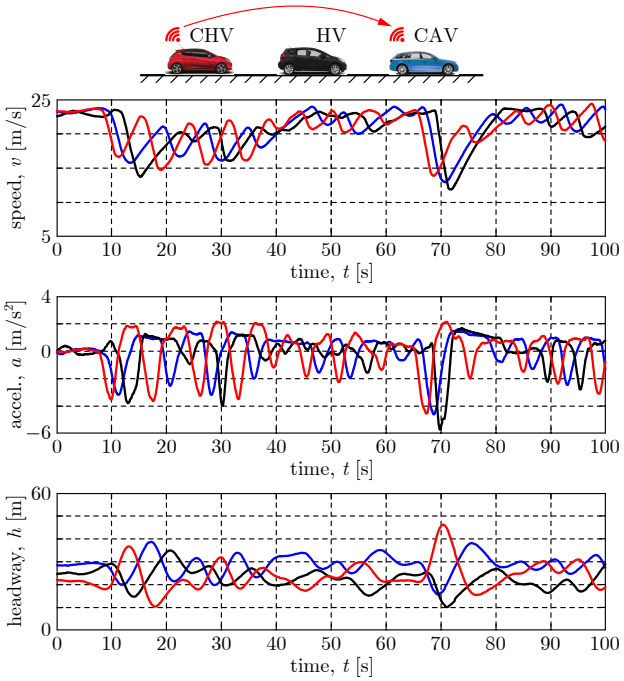

Fig. 6. Virtual ring experiment for virtual ring length $L + 3l = 90\,\mathrm{m}$ where the CAV responds to one CHV "ahead" while utilizing the controller (7,8,9) with free flow headway $h_{\mathrm{go}} = 35\,\mathrm{m}$. The red CHV imposes perturbations around $t = 10\,\mathrm{s}$ and $t = 65\,\mathrm{s}$ and in both cases limit cycle oscillations develop.

the blue CAV only responds to the red CHV "ahead", but the gradient of the CAV's range policy is increased by reducing the free flow headway to $h_{\mathrm{go},N} = 42.5\,\mathrm{m}$. This results in a smaller equilibrium headway for the CAV, and in turn, larger headways for the human-driven vehicles. Initially, the system stays close to the equilibrium until about $t = 10\,\mathrm{s}$ when the red CHV imposes a perturbation. The corresponding transients decay and the system returns to the equilibrium. This means that the equilibrium is locally stable. However, at $t = 35\,\mathrm{s}$ the red CHV imposes another, slightly larger perturbation, and the related transients grow into sustained oscillations. Similar to the theoretical results, the experiments reveal bistable behavior: the system either converges to the locally stable equilibrium or to the locally stable limit cycle depending on the applied perturbations. Although, the oscillation amplitude of the numerical analysis and the experiments are not the same, the corresponding time period of oscillations are in the same range as they are $T_{\mathrm{p,n}} \approx 12\,\mathrm{s}$ and $T_{\mathrm{p,e}} \approx 8\,\mathrm{s}$ in the numerical analysis and in the experiments, respectively.

In Fig. 6, the gradient of the range policy is increased further by decreasing the free flow headway to $h_{\mathrm{go},N} = 35\,\mathrm{m}$, while the CAV still utilizes the same control strategy as in Figs. 4 and 5. This further decreases the equilibrium headway of the CAV, and in turn, further increases the equilibrium headways of the human-driven vehicles. Again, perturbations, like those applied by the red CHV at $t = 10\,\mathrm{s}$ and $t = 65\,\mathrm{s}$, lead to sustained oscillations, while the system can still return to the equilibrium from time to time, indicating bistability. The fact that even smaller perturbations can trigger sustained oscillations suggests that the region of attraction of the equilibrium is smaller than it was in the $h_{\mathrm{go},N} = 42.5\,\mathrm{m}$ case.

Finally, in order to eliminate bistability, we change the control strategy as demonstrated in Fig. 7. Here, the CAV responds to the red CHV "ahead" as well as to the black CHV "two vehicles ahead" using the controller:

$$u_N = \alpha_N\big(V_N(h_N) - v_N\big) + \beta_{N,1}\big(W_N(v_1) - v_N\big) + \beta_{N,2}\big(W_N(v_2) - v_N\big)\,, \tag{13}$$

cf. (8). The free flow headway is set to $h_{\mathrm{go},N} = 35\,\mathrm{m}$, while the gains are $\alpha_N = 0.4\,\mathrm{s}^{-1}$, $\beta_{N,1} = 0.2\,\mathrm{s}^{-1}$ and $\beta_{N,2} = 0.3\,\mathrm{s}^{-1}$. In this case, the equilibrium becomes globally stable as shown by the decay of the oscillations triggered by the red CHV at $t = 35\,\mathrm{s}$ and $t = 75\,\mathrm{s}$. This demonstrates the benefits of V2X connectivity in stabilizing a system that is otherwise prone to limit cycle oscillations. Compared to Fig. 4, where the equilibrium was also globally stable, here the CAV is able to maintain smaller headways.

V. Conclusion

We analyzed the nonlinear dynamics of vehicles on a virtual ring created by vehicles traveling on a straight road such that the last CHV is "projected" ahead of the first CAV. This configuration allows one to carry out experiments with realistic speeds without the presence of large lateral (centrifugal) forces. In addition, it is also safer than a conventional ring configuration, because the CAV cannot run into the

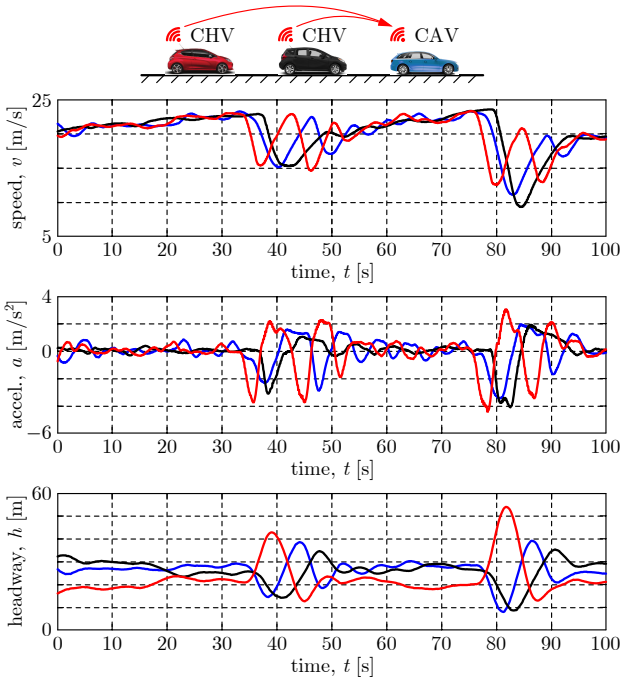

Fig. 7. Virtual ring experiment for virtual ring length $L + 3l = 90\,\mathrm{m}$ where the CAV responds to two CHVs "ahead" while utilizing the controller (7,9,13) with free flow headway $h_{\mathrm{go}} = 35\,\mathrm{m}$. The gain parameters are set to $\alpha_N = 0.4\,\mathrm{s}^{-1}$, $\beta_{N,1} = 0.2\,\mathrm{s}^{-1}$, $\beta_{N,2} = 0.3\,\mathrm{s}^{-1}$. The red CHV imposes perturbations around $t = 35\,\mathrm{s}$ and $t = 75\,\mathrm{s}$ and in both cases the system returns to the equilibrium after some transient oscillations.

vehicle "ahead" as it is not physically there. Via numerical bifurcation analysis, we showed that the system is bistable under certain parameter combinations even for 3 vehicles. Additionally, increasing the number of vehicles increases the bistable domain. We observed the same qualitative behavior by conducting experiments on a virtual ring with 3 commercial vehicles, one of which was turned into a CAV. The results confirmed the presence of bistability. Finally, when the CAV responded to the vehicle "two vehicles ahead"; this led to the most stable behavior with beneficially small headways. The results support the control design of CAVs, and provide new ways to mitigate phantom traffic jams.

In the future, we plan to carry out an extensive measurement campaign to discover the effects of various parameter combinations and large vehicle fleets, and to examine the dynamics in diverse environments. Besides, we plan to develop theoretical models of human driving behavior based on the measurement results. For this, there are already promising methods in the literature utilizing neural networks [23] or Bayesian inference algorithms [24].

References

[1] G. Orosz, R. E. Wilson, R. Szalai, and G. Stépán, "Exciting traffic jams: Nonlinear phenomena behind traffic jam formation on highways," *Physical Review E*, vol. 80, no. 4, p. 046205, 2009.

[2] T. G. Molnár and G. Orosz, "Destroying phantom jams with connectivity and automation: Nonlinear dynamics and control of mixed traffic," *Transportation Science*, vol. 58, no. 6, pp. 1319–1334, 2024.

[3] S. S. Avedisov, G. Bansal, and G. Orosz, "Impacts of connected automated vehicles on freeway traffic patterns at different penetration levels," *IEEE Transactions on Intelligent Transportation Systems*, vol. 23, no. 5, pp. 4305–4318, 2022.

[4] S. E. Shladover, D. Su, and X.-Y. Lu, "Impacts of cooperative adaptive cruise control on freeway traffic flow," *Transportation Research Record*, vol. 2324, no. 1, pp. 63–70, 2012.

[5] S. Öncü, J. Ploeg, N. van de Wouw, and H. Nijmeijer, "Cooperative adaptive cruise control: network-aware analysis of string stability," *IEEE Transaction on Intelligent Transportation Systems*, vol. 15, no. 4, pp. 1527–1537, 2014.

[6] Z. Wang, G. Wu, and M. J. Barth, "A review on cooperative adaptive cruise control (CACC) systems: Architectures, controls, and applications," in *21st IEEE International Conference on Intelligent Transportation Systems*. IEEE, 2018, pp. 2884–2891.

[7] G. Orosz, "Connected cruise control: modelling, delay effects, and nonlinear behaviour," *Vehicle System Dynamics*, vol. 54, no. 8, pp. 1147–1176, 2016.

[8] Y. Qin, H. Wang, and B. Ran, "Control design for stable connected cruise control systems to enhance safety and traffic efficiency," *IET Intelligent Transport Systems*, vol. 12, no. 8, pp. 921–930, 2018.

[9] J. I. Ge and G. Orosz, "Connected cruise control among human-driven vehicles: Experiment-based parameter estimation and optimal control design," *Transportation Research Part C*, vol. 95, pp. 445–459, 2018.

[10] T. G. Molnár, M. Hopka, D. Upadhyay, M. Van Nieuwstadt, and G. Orosz, "Virtual rings on highways: Traffic control by connected automated vehicles," in *AI-enabled Technologies for Autonomous and Connected Vehicles*. Springer, 2023, pp. 441–479.

[11] S. Guo, G. Orosz, and T. G. Molnár, "Connected cruise and traffic control for pairs of connected automated vehicles," *IEEE Transactions on Intelligent Transportation Systems*, vol. 24, no. 11, pp. 12 648–12 658, 2023.

[12] Y. Sugiyama, M. Fukui, M. Kikuchi, K. Hasebe, A. Nakayama, K. Nishinari, S.-i. Tadaki, and S. Yukawa, "Traffic jams without bottlenecks – experimental evidence for the physical mechanism of the formation of a jam," *New Journal of Physics*, vol. 10, no. 3, p. 033001, 2008.

[13] Y. Zheng, J. Wang, and K. Li, "Smoothing traffic flow via control of autonomous vehicles," *IEEE Internet of Things Journal*, vol. 7, no. 5, pp. 3882–3896, 2020.

[14] M. Pooladsanj, K. Savla, and P. A. Ioannou, "Vehicle following on a ring road under safety constraints: Role of connectivity and coordination," *IEEE Transactions on Intelligent Vehicles*, vol. 8, no. 1, pp. 628–638, 2022.

[15] R. E. Stern, S. Cui, M. L. Delle Monache, R. Bhadani, M. Bunting, M. Churchill, N. Hamilton, R. Haulcy, H. Pohlmann, F. Wu, B. Piccoli, B. Seibold, J. Sprinkle, and D. B. Work, "Dissipation of stop-and-go waves via control of autonomous vehicles: Field experiments," *Transportation Research Part C*, vol. 89, pp. 205–221, 2018.

[16] M. Bando, K. Hasebe, K. Nakanishi, and A. Nakayama, "Analysis of optimal velocity model with explicit delay," *Physical Review E*, vol. 58, no. 5, pp. 5429–5435, 1998.

[17] M. Bando, K. Hasebe, A. Nakayama, A. Shibata, and Y. Sugiyama, "Dynamical model of traffic congestion and numerical simulation," *Physical Review E*, vol. 51, no. 2, pp. 1035–1042, 1995.

[18] K. Engelborghs, T. Luzyanina, and D. Roose, "Numerical bifurcation analysis of delay differential equations using DDE-BIFTOOL," *ACM Transactions on Mathematical Software*, vol. 28, no. 1, pp. 1–21, 2002.

[19] Y. Wang, M. L. Delle Monache, and D. B. Work, "Identifiability of car-following dynamics," *Physica D*, vol. 430, p. 133090, 2022.

[20] N. Bekiaris-Liberis, "Nonlinear predictor-feedback cooperative adaptive cruise control of vehicles with nonlinear dynamics and input delay," *International Journal of Robust and Nonlinear Control*, vol. 34, no. 10, pp. 6683–6698, 2024.

[21] R. De Haan, T. van der Sande, E. Lefeber, and I. Besselink, "Cooperative adaptive cruise control for heterogeneous platoons with delays: Controller design and experiments," *IEEE Transactions on Control Systems Technology*, 2024.

[22] J. Inman, *Navigation and Nautical Astronomy: For the Use of British Seamen*. C. W. Woodward and J. Rivington, 1835.

[23] X. A. Ji and G. Orosz, "Trainable delays in time delay neural networks for learning delayed dynamics," *IEEE Transactions on Neural Networks and Learning Systems*, 2024.

[24] X. A. Ji, T. G. Molnár, A. A. Gorodetsky, and G. Orosz, "Bayesian inference for time delay systems with application to connected automated vehicles," in *24th IEEE International Conference on Intelligent Transportation Systems*. IEEE, 2021, pp. 3259–3264.